Journal of Universal Computer Science, vol. 16, no. 10 (2010), 1327-1342
submitted: 19/7/08, accepted: 9/3/10, appeared: 28/5/10 © *J.UCS*

Gabor Filter Aided 3D Ultra-Sonography Diagnosis System with WLAN Transmission Consideration

Wei-Ming Chen
(Institute of Computer Science & Information Engineering, National Ilan University, I-Lan Taiwan, ROC
wmchen@niu.edu.tw)

Chi-Hsiang Lo
(Department of Electronic Engineering, National Ilan University, I-Lan, Taiwan, ROC
chlo@niu.edu.tw)

Han-Chieh Chao
(Institute of Computer Science & Information Engineering, National Ilan University, I-Lan Taiwan, ROC
Department of Electronic Engineering, National Ilan University, I-Lan, Taiwan, ROC
Department of Electrical Engineering, National Dong Hwa University, Hualien, Taiwan, ROC
hcc@niu.edu.tw)

Chun-Cheng Chang
(Department of Electrical Engineering, National Dong Hwa University, Hualien, Taiwan, ROC
aziz0916@yahoo.com.tw)

Abstract: The Gabor filter aided diagnosis system for 3-dimensional ultra-sonography (3DUS) under the WLAN environment is introduced. Due to the important relationship between breast tumour surface features and internal architecture, we applied our system using 3D inter-pixel correlations instead of 2D features. Gabor filters provide a multi-resolution representation of texture, which increases ultrasound technology capability in the differential diagnosis of solid breast tumours. Our experiments show that the performance of the proposed diagnostic method is effective. Moreover, physicians manipulate our diagnostic system using hand-held devices in the hospital. Because WLAN is unstable, our system ensures good transmission quality. We also focus on transmission control strategies that adapt to the time varying wireless network conditions. We analyze strategies that use competitive analysis techniques. The experiments show that the algorithm's performance is effective.

Keywords: 3D ultrasound, 3DUS, breast tumour, speckle noise, Gabor filter, auto-correlation, neural network, WLAN Transmission
Categories: SD I.4.0

1 Introduction

The ultrasound (US) imaging system is widely used in hospitals, physicians' offices and clinics. Since the traditional 2D ultrasound (2DUS) cannot easily demonstrate tumour surface features and internal architecture simultaneously, the 3D ultrasound (3DUS) has been developed. The physician can now view the construction in 3D

[Chen et al. 2003a], [Chang et al. 2003], [Chen et al. 2003b], [Sallout et al. 2006]. A 3D object, such as a breast tumour, usually has volume and appears as an uneven complex shape. In 2DUS, if the 2D probe is not located at the correct location or the scanned 2D image contains only partial tumour features, it may result in a misdiagnosis. Because the 3DUS reduces the variability, it could be a potentially reliable diagnostic tool for solid breast tumour analysis. The pixel relation analysis techniques are useful in diagnosing breast lesions. Only one single 2D data slice was used for each case in the conventional 2DUS diagnostic system. When the diagnostic features come from only one slice, that slice may fail to represent all of the tumour's diagnostic features. For these reasons, 3DUS datasets are used in this paper.

Texture analysis is essential in distinguishing speckled noise from meaningful tissue texture produced by US imaging [Goncalves et al. 2006]. Texture analysis algorithms range from random field models to multi-resolution filtering techniques [Lee and Shi 2009]. We propose a multi-resolution representation method based on the Gabor filters. Gabor filters have been used in several image analysis applications including texture classification and segmentation [Bovic et al. 1990], [Manjunath and Chellappa 1993], image recognition [Daugman 1993], [Lades 1993], [Manjunath and Chellappa 1992], image registration and motion tracking [Manjunath et al. 1996]. Most of these researches are related to texture segmentation and analysis. Gabor filters are used in this research to extract textured image features using various factors, which improve image resolution, orientation selectivity and spatial frequency tuning. The Gabor approach can achieve optimal resolution in both space and spatial frequency. Using the appropriate filters with the optimal parameters to increase the computational efficiency and extract more meaningful information, we propose using the texture parameters to compute the auto-correlation matrix as the characteristic vector in our artificial neural network diagnosis models as well. The region of interest (ROI) and volume of interest (VOI) of the US images are located by physicians.

Because physicians can manipulate this system using hand-held devices in the hospital, every transmission between the system and physicians is under WLAN. Like any radio frequency transmission, wireless networking signals are subject to a wide variety of interference, as well as complex propagation effects that are beyond the control of the network administrator. The environment for transmission may be lost or produce errors within the bandwidth limits.

In order to extract the sub-images of VOI, three tumour regions need to be sketched by the physician under WLAN. The image-data quality under the wireless transmission will affect the sketch result. In other words, it may affect the diagnostic accuracy. A very reliable communication system is required to support our system. Transmission methods that avoid the failure caused by lost or errant packets are therefore very important in order to provide reliable communication. We also focus on the transmission control strategies that adapt to the time varying wireless network conditions. These algorithms can employ a number of strategies. For example, blindly estimating the channel state, employing a channel predictor to obtain information about the state of the wireless channel, estimating the probability distribution of the channel state variation, or using non-adaptive and adaptive threshold schemes to decide when to transmit and when to stop. Here we consider the last approach.

Moreover, we analyze strategies that use competitive analysis techniques. The previous proposed competitive analysis shows how good the link layer transmission control algorithms are compared with the optimal algorithm that has perfect knowledge of the wireless channel states for the entire duration of the transmission. In fact, the optimal algorithm is not practical. We assume that packet losses are solely due to physical imperfections in the wireless channel, i.e., we neglect other interferences such as multi-user interference, etc., for the sake of simplicity [Sleator and Tarjan 1985], [Chandramouli et al. 2004].

In Section 2, we introduce the computer-aided diagnosis system. Section 3 shows the transmission algorithms. Our conclusion is discussed in the last section.

2 Computer-aided diagnosis system

2.1 Materials and Methods

Speckle Noise

The speckle is a type of noise that changes the tissue parameters. It is a phenomenon caused when a coherent imaging system, such as US, is used to image a surface that is rough on the wavelength scale used. The surface produces many reflections in each resolution cell that adds constructively or destructively to produce a speckled pattern. A US speckled image has the magnitude of a complex Gaussian field with independent real and imaginary parts that are distributed identically [Czerwinski et al. 1994].

A small amount of additive noise might be shown in US scans. An image may be classified as possessing Gaussian noise with a very small standard deviation into different levels of speckled noise. The p(x) (Zero-mean Gaussian noise also represents the speckle noise) with standard deviation σ is drawn from the probability density function

$$p(x) = \frac{1}{\sqrt{2\pi} \cdot \sigma} \exp(-\frac{x^2}{2\sigma^2})$$

(1)

where x denotes the grey level of the uncorrupted image [Wachowiak et al. 2000].

Gabor Filters

2-D Gabor function is a Gaussian modulated by a complex sinusoidal plane wave of some frequency and orientation. The general form for the 2-D Gabor function is given by

$$G(x, y) = g(x, y) \cdot \exp[2\pi i(Ux + Vy)]$$

(2)

where $i = \sqrt{-1}, U = F\cos\theta, V = F\sin\theta,$ and F=1/T (T is period), g(x,y) is 2-D Gaussian function given by

$$g(x, y) = \frac{1}{2\pi\sigma^2} \exp[-(\frac{x^2}{2\sigma_x^2} + \frac{y^2}{2\sigma_y^2})]$$

(3)

with σ is standard deviation. From Eq. (2) and (3), and by applying the Euler identity, Eq. (2) can be rewritten as [Dantas and Costa 2007]

$$G(x, y) = \frac{1}{2\pi\sigma^2} \exp[-(\frac{x^2 + y^2}{2\sigma^2})] \cdot$$
$$\{\cos[2\pi(Ux + Vy)] + i \sin[2\pi(Ux + Vy)]\}$$

(4)

Because Gabor filters are used to extract meaningful features from real images, the response to the even-symmetrical filter components will remain unchanged for filters oriented 180º out of phase and the odd-symmetrical component will be negated [Jähne 1997]. Therefore, our proposed Gabor function representation uses only real-valued, even symmetrical filters oriented over a 180º range as opposed to the full 360º range commonly described in the literature.

Auto-correlation Function

The correlation between neighbouring pixels within the 3D images is a patent feature of a tumour. The normalized auto-correlation coefficients [Jähne 1997] are used to reflect the inter-pixel correlation within an image. The 3D normalized auto-correlation coefficients can be defined as

$$r(\Delta m, \Delta n, \Delta p) = \frac{A(\Delta m, \Delta n, \Delta p)}{A(0,0,0)}$$

(5)

where

$$A(\Delta m, \Delta n, \Delta p) = \frac{1}{(M - \Delta m)(N - \Delta n)(P - \Delta p)} \sum_{x=0}^{M-1-\Delta m} \sum_{y=0}^{N-1-\Delta n}$$
$$\sum_{z=0}^{P-1-\Delta p} f(x, y, z) f(x + \Delta m, y + \Delta n, z + \Delta p)$$

(6)

where r(Δm,Δn,Δp) is the normalized auto-correlation coefficient between pixel (x,y,z) and pixel (x+Δm,y+Δn,z+Δp) in an image with size M × N × P.

Neural Networks

Neural networks have been applied in the image processing field to solve classification, recognition, prediction or compression problems. Neural networks consist of simple computing units, called neurons or processing units, and the massive interconnections between these units.

We used the feed-forward neural network in this research. These components are valid whether the neuron is used for input, output, or is in one of the hidden layers. Neurons are organized into layers, called neuron layers, and the neuron layers would constitute neural networks. Figure 2 shows a feed-forward neural network example with three neuron layers (one input layer, one output layer and one hidden layer).

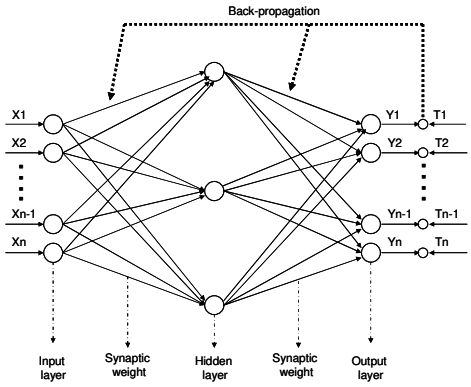

Figure 1: A feed-forward neural network with three neuron layers

2.2 Experiments and Results

Figure 2 shows the overall proposed method. At the first, rough sub-images of the volume of interest (VOI) are determined by a physician under WLAN environment. System will extract the VOI-array from the 3DUS image by the three regions (ROI) which sketched by physicians.

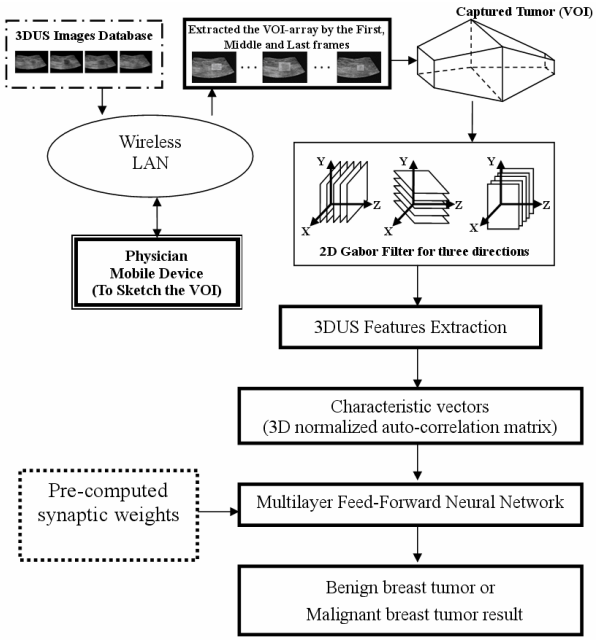

Figure 2: The proposed system

After that, several Gabor filters with different directions and frequencies are used to eliminate the speckled noise and extract meaningful features from VOI-array. The 3DUS features are then generated by the 3D auto-correlation function. These 3DUS features will be formed as a characteristic vector. These characteristic vectors were further fed into the source nodes in the input layer of the multilayer feed-forward neural network. When the performance is sub-optimal for new 3DUS images, these images will be added into the original training set again to reproduce a new set of synaptic weight vectors by adjusting the free parameters. The value produced by the output layer is used to decide whether the tumour is benign or malignant.

The overall performance of the process was evaluated on 107 cases of malignant and 54 cases of benign tumours. The 3DUS imaging was performed using a Voluson 530 (Kretz Technik, Zipf, Austria) scanner and a Voluson small part transducer S-VNW5 to 10. Figure 3 is the 2D image planes arranged in a fanlike geometry.

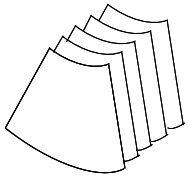

Figure 3: A fanlike geometry

Figure 4 shows three fixed axes of 3DUS. The three fixed directions are used for the 2D Gabor filter process.

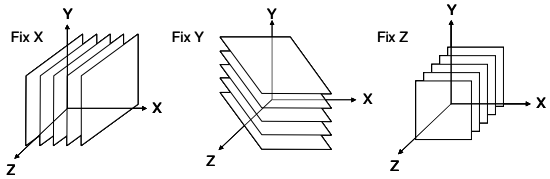

Figure 4: Three fixed axes for the 2D Gabor filter process

Figure 5 shows that the speckled noise has apparently been reduced. A 3DUS image combined using a series of 2D slices will therefore be improved.

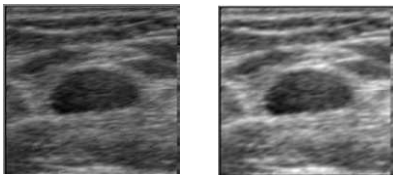

Figure 5: (a) is the original 2S ultrasound image and (b) is the 2D ultrasound image after the processor of Gabor filters

We also defined four variables to measure the performance. TN is the number of benign cases diagnosed correctly. FP is the number of benign cases that were misdiagnosed. TP is the number of malignant cases diagnosed correctly and FN is the number of malignant cases misdiagnosed.

Several measurements are defined as follows:

Accuracy = (TP+TN) / (TP+TN+FP+FN)
Sensitivity = TP / (TP+FN)
Specificity = TN / (TN+FP)
Positive Predictive Value = TP / (TP+FP)
Negative Predictive Value = TN / (TN+FN)

The performance between the origin and Z_45_T_6 are compared in Tables 1 and 2. In Table 1, the FP between proposed method (Z_45_T_6) and origin decreases to 4.

Sonographic Classification	Proposed method (Z_45_T_6)		Origin (AC-3DUS without Gabor Filters)	
	Begin	Malignant	Begin	Malignant
Begin	TN96	FN1	TN92	FN1
Malignant	FP4	TP47	FP8	TP47
Total	100	48	100	48

Table 1: Classification of the breast nodules by proposed method (at threshold = 0.5) and AC-3DUS without Gabor Filters (at threshold = 0.5)

Item	Proposed method (Z_45_T_6)	Origin (AC-3DUS without Gabor Filters)
Accuracy (%)	96.6	93.9
Sensitivity (%)	97.9	97.9
Specificity (%)	96.0	92.0
Positive Predictive Value (%)	92.2	85.5
Negative Predictive Value (%)	99.0	98.9

Table 2: Performance comparison of the proposed method (Z_45_T_6) and AC-3DUS without Gabor Filters

In Figure 6, the receiver operating characteristic curve (ROC) is shown to represent the diagnostic performance. FPF stands for false-positive fraction and the TPF is the value of the true-positive fraction. The curve showing the abrupt jump (the value of FPF is closer to 0 while the value of the TPF arrives at 1) should be the better one.

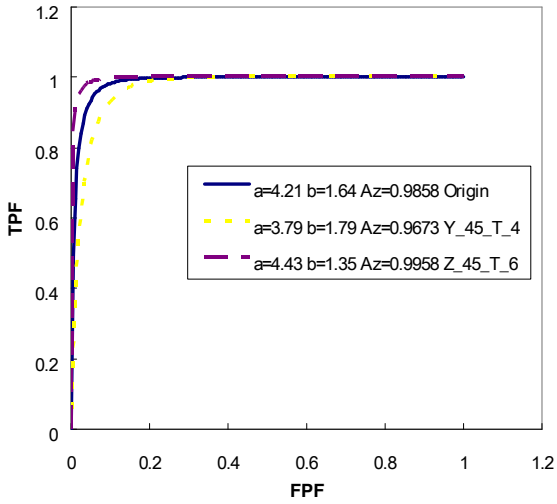

Figure 6. Conventional ROC curves of origin, Y_45_T_4 and Z_45_T_6

The accuracy, sensitivity, specificity, PPV (positive predictive value) and NPV (negative predictive value) for the diagnostic performance are clearly demonstrated in Figure 7. Figure 7 shows the performance of the Z axis was better than that for the X and Y axes. For the Z axis, the case is better than others which the angle (θ) is 45° and the period (T) is 6.

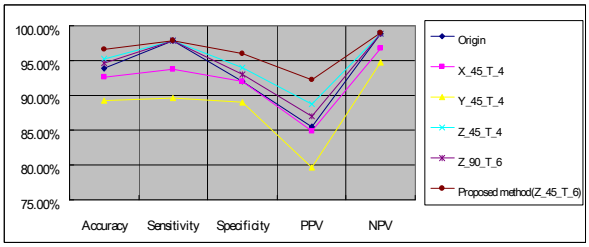

Figure 7: The accuracy, sensitivity, specificity, PPV and NPV for diagnostic performance

3 WLAN Transmission algorithms

Section 2 discusses how we can obtain meaningful diagnostic information using the diagnosis system. However, every transmission between the system and physicians occurs under a WLAN environment[Chang et al. 2007][Mahani et al. 2009]. Incorrect 3DUS image transmission will cause physicians to make a wrong ROI sketch result, or a wrong judgment. This situation will also affect the diagnostic accuracy. The transmission algorithm must ensure that every image data are transmitted

appropriately. In this section, we will discuss the transmission algorithms for our system.

Competitive analysis is concerned with comparing the performance of on-line algorithms with that of an optimal off-line algorithm. There is an algorithm *A* which is said to be *c*-competitive if for any fixed input sequence σ ,

$$EC_A(\sigma) \le c \cdot C_{opt}(\sigma) \tag{7}$$

where $EC_A(\sigma)$ is the expected cost, A incurs when the processing input sequence σ and $C_{opt}(\sigma)$ is the cost incurred by the optimal off-line algorithm in processingσ . We use two different algorithms in this paper to solve the channel adaptive image transmission problem [Chandramouli et al. 2004], [Gonzalez and Woods 1992], [Borodin and El-Yaniv 1998], [Chandramouli and Uma 2003]:

Deterministic algorithm

Assume E_t is the energy dissipated in transmitting one packet using the mobile unit and E_d is the energy dissipated during T_o time units where T_o is the time-out period after which the mobile unit will resume transmission. Let

$$r = \lceil E_d / E_t \rceil \tag{8}$$

where $r \ge 1$ without loss of generality. The on-line algorithm, denoted A_r, is as follows:

Algorithm **Deterministic:**
If number of consecutive packets lost $\ge r$
{stop transmission
restart transmission after T_o time units}.

Because it realizes that the channel condition is bad only after losing r consecutive packets. Therefore, the over all cost is the cost of transmitting the r packets plus the delay incurred because of the time-out. Conversely, the optimal off-line algorithm knows in advance that the channel is bad and will not waste energy in transmitting these r packets. The cost it incurs is only the cost due to time-out. For this reason, we have $EC_A(\sigma)=2 \cdot C_{opt}(\sigma)$. Or say, ***c*** is a constant 2 in equation (7). Therefore, the Deterministic algorithm, A_r is 2-competitive. The advantage of Deterministic is less delay time, but it loses more packets.

Randomized algorithm

Assume σ_x is an input sequence of channel states and A_i is the deterministic algorithm with threshold i. The randomized algorithm A chooses algorithm A_i with a probability π_i.

Algorithm **Randomized:**

Let A_i be the algorithm Deterministic with threshold π_i.

Choose A_i with probability π_i.

The stop time equation T_o is

$$T_o = \lambda v \tag{9}$$

where λ is a constant and v is the time taken to transmit one packet. We assume that

$$E_q = \mu E_t \tag{10}$$

$$E_d = \lambda E_q \tag{11}$$

where E_q is the unit of energy to transmit one packet during T_o and μ is a constant. From equation (8), (10), and (11), we obtain the following:

$$\lambda = r/\mu \tag{12}$$

We observe that the expected cost of randomized algorithm A on sequence σ_x is

$$EC_A(\sigma_x) = \sum_{1 \le i \le x} \pi_i (iE_t + E_d) + (1 - \sum_{1 \le i \le x} \pi_i) xE_t \tag{13}$$

Then obtaining a family of equations by setting $x = 1,2,3,\ldots$. Solving the resulting difference equations gives

$$\pi_i = \begin{cases} \dfrac{\alpha}{r}\left(\dfrac{r+1}{r}\right)^{i-1} & i = 1,2,\ldots,r \\ 0 & otherwise \end{cases} \tag{14}$$

Solving for α by setting $\sum_{1 \le i \le r} \pi_i = 1$, we get $\alpha = \dfrac{1}{(1+\frac{1}{r})^r - 1}$ (15)

Taking limit $r \to \infty$ of the competitive ratio $(1+\alpha)$ yields

$$\frac{e}{e-1} \tag{16}$$

Therefore, we get the randomized algorithm has a competitive ratio with equation (16).

The advantage of Randomized is less packet losses than Deterministic algorithm, but it uses more delay time.

$$E(C_A(\sigma_x)) = \sum_{1 \le i \le x} \pi_i (iE_t + E_d) + (1 - \sum_{1 \le i \le x} \pi_i) xE_t$$

The above is shown in Fig. 8.

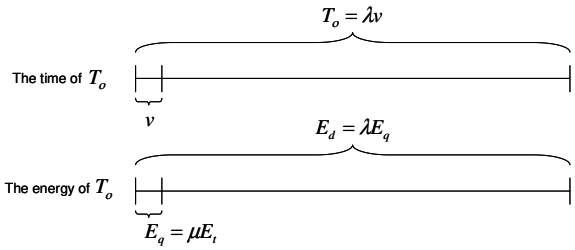

Figure 8: The time and energy of T_o

3.1 Transmission conditions

Each 3DUS image case should be decomposed into 2DUS image frames and be transmitted to the physicians respectively. The transmission algorithms could be discussed in three conditions.

1. The 3D ultrasound image frames without ROI (region of interest sketched bt the physician). The frames without ROI are not really important. They are shown as a reference for the physician and may not affect the diagnostic accuracy. We employ the Randomized algorithm to transmit the image frame to reduce the packets loss.
2. The 3D ultrasound image frames within ROI. Because the ROI packets that contain the whole tumour information are more important than others and cannot be lost, it will affect the diagnostic accuracy. We use the Randomized algorithm to transmit the ROI part and the Deterministic algorithm to transmit the other parts.
3. In our system, there are only a few frames within the ROI after the physician sketch process. The system must then exploit these frames to estimate the other ROI in the frames not sketched but containing tumor information. In this case, we selected method of **2**.

The method to find the frames which are not ROI sketched is discussed later. Generally, there are fifty-four 2D ultrasound slices that should be sketched to grab the whole tumour, or VOI. The ROI of the middle frame is generally the biggest, as shown in Figure 9.

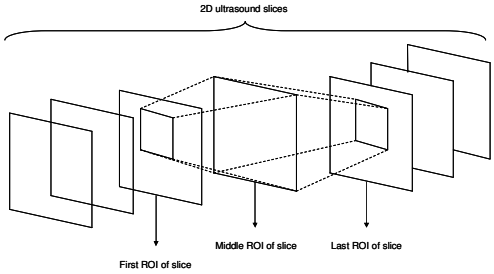

Figure 9: The ROI of 2D ultrasound slices

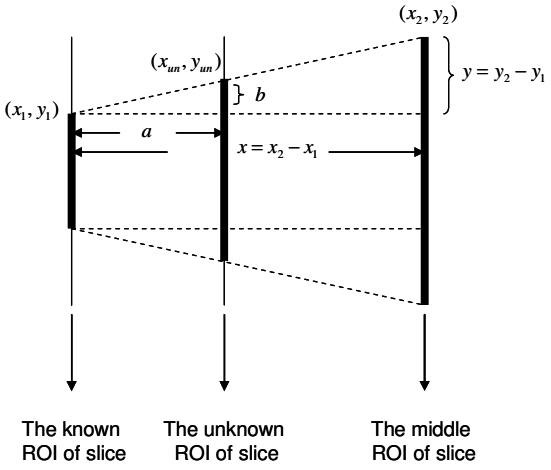

Figure 10: The coordinate of unknown ROI of 2D ultrasound slice

The coordinate of unknown ROI for the 2D ultrasound slice is computed in Figure 10 and equation (17).

$$\begin{aligned} x_{un} &= x_1 + a \\ y_{un} &= y_1 + b \\ b &= ay/x \end{aligned} \tag{17}$$

where a is the number of unknown ROI slices. The other unknown ROI coordinates for the 2D ultrasound slices are also computed.

3.2 Experiments

Each 2D ultrasound image frame in 3DUS image is subdivided into 26×26 blocks and the resolution of each block is 8×8. Every block of the ultrasound images is encoded and decoded using the lossless DCT (discrete cosine transform). For the 2D

ultrasound image frames containing ROI, the packets with ROI pixels are transmitted first and the others are transmitted using the circle sequence from the inside to the outside. For the 2D ultrasound image frames without ROI, the packets are transmitted using the circle sequence from the centre to the edge. For the frames containing tumour information but no ROI sketch, our system will assume that their ROI is located at the centre by default. The reason is to avoid losing the important packets.

The ultrasound images are transmitted under two channel conditions (40% and 80%). The channel with higher value means it is busier than a smaller value. The coefficient μ is assumed 0.1 and γ is 3.

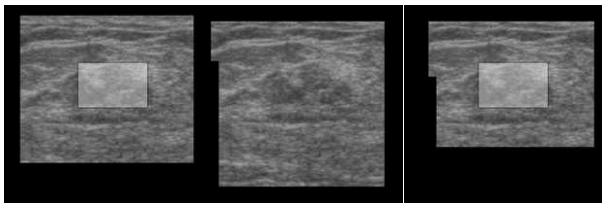

Figure 11: The transmitted ultrasound image with cancer are in three conditions (a) with ROI (using Randomized and Deterministic), (b) without ROI (using Randomized) and (c) with ROI (not using any transmission algorithms). The channel condition is 40%, the T_o is 30 and the γ is 3

	Energy	**Delay**	**Avg. packet loss**	**Packet loss rate**	**PSNR**
(a) with ROI (using randomized and deterministic)	**894.90E_t**	**2189**	**207**	**30.62%**	**13.66**
(b) without ROI (using randomized)	**1021.00E_t**	**3450**	**179**	**26.48%**	**14.27**
(c) with ROI (not using any transmission algorithm)	**676.00E_t**	**0**	**298**	**44.08%**	**11.88**
E_t : It is the energy dissipated in transmitting one packet by the mobile unit					

Table 3: The energy, delay, average packet loss, packet loss rate and PSNR of three conditions. The channel condition is 40%, the T_o is 30 and theγ is 3

We randomly select forty 3DUS cases and each case transmits four 2DUS image frames to evaluate the algorithm performance. Figures 11 and 12 show the ultrasound images with cancer are transmitted in three conditions; with ROI (using Randomized and Deterministic), without ROI (using Randomized) and with ROI (not using any

transmission algorithms) and different channel conditions. Tables 3 and 4 show the energy, delay, average packet loss, packet loss rate and PSNR (peak signal to noise ratio) of three conditions with different channel conditions.

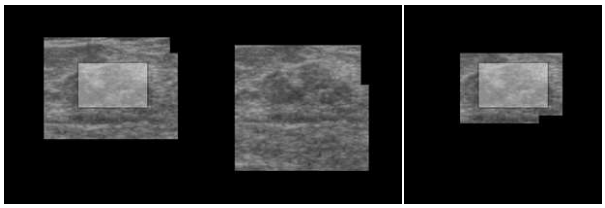

Figure 12: The ultrasound image with cancer are transmitted in three conditions which are (a) with ROI (using Randomized and Deterministic), (b) without ROI (using Randomized) and (c) with ROI (not using any transmission algorithms). The channel condition is 80%, the T_o is 30 and the γ is 3

	Energy	Delay	Avg. packet loss	Packet loss rate	PSNR
(a) with ROI (using randomized and deterministic)	**1118.80E_t**	**4428**	**406**	**60.06%**	**10.29**
(b) without ROI (using randomized)	**1618.00E_t**	**9420**	**358**	**52.96%**	**10.78**
(c) with ROI (not using any transmission algorithm)	**676.00E_t**	**0**	**511**	**75.59%**	**9.04**
E_t : It is the energy dissipated in transmitting one packet by the mobile unit					

Table 4: The energy, delay, average packet loss, packet loss rate and PSNR of three conditions. The channel condition is 80%, the T_o is 30 and the γ is 3

4 Conclusion

We bring forward a new method for reducing speckled noise using Gabor filters in 3DUS images. The feed forward neural network diagnostic system adopting 3D inter-pixel correlation features is used instead of 2D features to obtain a better result. We focused on processes involving scanning, pixel extraction, texture analysis, and auto-correlation calculation. The Gabor filters provided multiple orientations and multiple scales, which are the desired texture analysis properties.

After our system obtains better diagnostic accuracy it still requires a stable wireless network environment. From section 3, ultrasound images are transmitted using Randomized and Deterministic algorithms. The ultrasound images with ROI transmitted by Randomized and Deterministic algorithms can reduce packet loss, but

increase the energy and delay. The ultrasound images without ROI transmitted using Randomized algorithms can reduce the energy and delay, but increase packet loss. Although the ultrasound images with ROI transmitted without any transmission algorithms can reduce the energy and delay, the packet loss rate is not acceptable. It will affect the diagnostic accuracy. Therefore, transmitting ultrasound images using Randomized and Deterministic algorithms under different conditions is suggested.

Acknowledgements

This paper is a partial result of project no 96-2218-E-002-007- & NSC 96-2221-E-197-024- conducted by the National Ilan University under the sponsorship of National Science Council, Taiwan, ROC.

References

[Borodin and El-Yaniv 1998] Borodin, A. and El-Yaniv, R.: "Online computation and competitive analysis"; Cambridge University Press, 1998.

[Bovic et al. 1990] Bovic, A.C., Clark, M. and Geisler, W.S.: "Multichannel Texture Analysis Using Localized Spatial Filters"; IEEE Trans. Pattern Analysis and Machine Intelligence, vol. 12, no. 1, Jan. 1990, pp. 55-73.

[Chandramouli and Uma 2003] Chandramouli, R. and Uma, R. N., "To transmit or not to transmit: An investigation using competitive analysis"; Proceedings of the IEEE Wireless Communications and Networking Conference, 2003.

[Chandramouli et al. 2004] Chandramouli, R., Kumar, S. S. G. V. and Uma, R. N.: "Energy-Aware On-Line Algorithms for Image Transmission over Wireless LAN"; IEEE Communications Society, pp. 1350-1354, 2004.

[Chang et al. 2007] Chang, C. Y., Wu, T. Y., Huang,C. C., Whang, J. W. and Chao, H. C.: " Robust Header Compression with Load Balance and Dynamic Bandwidth Aggregation Capabilities in WLAN," Journal of Internet Technology, vol. 8, no. 3, July 2007, pp. 365-372.

[Chang et al. 2003] Chang, R. F., Wu, W. J., Chen, D. R., Chen, W. M., Shu, W. and Lee, J. H.: "3D US Frame Positioning Using Speckle Decorrelation and Image Matching"; Ultrasound in Medicine and Biology, vol. 29, no. 6, June 2003, pp. 801-812.

[Chen et al. 2003a] Chen, D. R., Chang R. F., Chen, W. M. and Moon, W. K.: "Computer Aided Diagnosis for 3-Dimensional Breast Ultrasonography," Archives of Surgery, vol. 138, no. 3, March 2003, pp. 296-302.

[Chen et al. 2003b] Chen, W. M., Chang, R. F., Moon M. K. and Chen, D. R.: "Breast Cancer Diagnosis Using Three Dimensional Ultrasound and Pixel Relation Analysis"; Ultrasound in Medicine and Biology, vol. 29, no. 7, July 2003, pp. 1027-1035.

[Czerwinski et al. 1994] Czerwinski, R.N., Jones, D.L., O'Brien, W.D., Jr.: "Edge Detection in Ultrasound Speckle Noise"; IEEE International Conf. ICIP-94, vol. 3, Nov. 1994, pp. 304-308.

[Dantas and Costa 2007] Dantas, R.G., Costa, E.T.: "Ultrasound Speckle Reduction Using Modified Gabor Filters"; IEEE Transactions on Ultrasonics, Ferroelectrics and Frequency Contro, vol. 54, no. 3, 2007, pp. 530-538.

[Daugman 1993] Daugman, J.G.: "High Confidence Visual Recognition of Persons by a Test of Statistical Independence"; IEEE Trans. Pattern Analysis and Machine Intelligence, vol. 15, no. 11, Nov. 1993, pp. 1,148-1,161.

[Goncalves et al. 2006] Goncalves, L. F., Nien, J. K., Espinoza, J., Kusanovic, J. P., Lee, W., Swope, B., Soto, E., Treadwell, M. C. and Romero, R.: "What Does 2-Doemensional Imaging Add to 3- and 4-Dimensional Obstetric Ultrasonography?"; Journal of Ultrasound in Medicine, vol. 25, no. 6, June 2006, pp. 691-699.

[Gonzalez and Woods 1992] Gonzalez, R.C. and Woods, R.E.: "Image Compression"; Digital image processing. Reading, Massachusetts, Addison Wesley, 1992, pp. 312-315.

[Jähne 1997] B. Jähne: "Digital Image Processing"; 4th ed. San Diego, CA : Springer, 1997.

[Lades 1993] Lades, M. et al.: "Distortion Invariant Object Recognition in the Dynamic Link Architecture," IEEE Trans. Computers, vol. 42, no. 3, Mar. 1993, pp. 300-311.

[Lee and Shi 2009] Lee, Jiann-Shu, and Shi, Yen-Ru: "A Mobile Phone Based Rock Classification System"; vol. 10, no. 3, July 2009, pp. 291-297.

[Mahani et al. 2009] Mahani, A. K, Rashvand, H. F., Teimoury, E., Naderi, M. and Abolhassani, B.: Wireless Mesh Networks Channel Reservation: Modelling and Delay Analysis", IET Communications, vol. 3, no. 5, May 2009, pp. 772-783.

[Manjunath and Chellappa 1992] Manjunath and Chellappa, R.: "A Feature Based Approach to Face Recognition"; Proc. IEEE Conf. CVPR '92, June 1992, pp. 373-378, Champaign, III..

[Manjunath and Chellappa 1993] Manjunath, B.S. and Chellappa, R.: "A Unified Approach to Boundary Detection"; IEEE Trans. Neural Networks, vol. 4,no. 1, Jan. 1993, pp. 96-108.

[Manjunath et al. 1996] Manjunath, Shekhar, C. and Chellappa, R.: "A New Approach to Image Feature Detection with Applications"; Pattern Recognition Volume 29, Issue 4, April 1996, pp. 627-640.

[Sallout et al. 2006] Sallout, B. I., D'Agostini, D. A. and Pretorius, D. H.: "Prental Diagnosis of Spondylocostal Dysotosis with 3-Dimensional Ultrasonography"; Journal of Ultrasound in Medicine, vol. 25, no. 4, April 2006, pp. 539-543.

[Sleator and Tarjan 1985] Sleator, D. D. and Tarjan, R. E.: "Amortized efficiency of list update and paging rules"; Communications of the ACM, Volume. 28, Issue 2, 1985, pp. 202-208.

[Wachowiak et al. 2000] Wachowiak, M.P., Elmaghraby, A.S., Smolikova, R., Zurada, J.M.: "Classification and Estimation of Ultrasound Speckle Noise with Neural Networks"; IEEE International Symposium on Bio-Informatics and Biomedical Engineering, 8-10, Nov. 2000, pp. 245-252.